Publication Year	2020
Acceptance in OA	2025-02-20T11:52:51Z
Title	Kinetic Simulations of the Jovian Energetic Ion Circulation around Ganymede
Authors	PLAINAKI, CHRISTINA, MASSETTI, Stefano, Jia, X., MURA, Alessandro, MILILLO, Anna, GRASSI, Davide, Sindoni, G., D'AVERSA, EMILIANO, FILACCHIONE, GIANRICO
Publisher's version (DOI)	10.3847/1538-4357/aba94c
Handle	http://hdl.handle.net/20.500.12386/36110
Journal	THE ASTROPHYSICAL JOURNAL
Volume	900

Manuscript submitted for publication in ApJ

Kinetic simulations of the Jovian energetic ion circulation around Ganymede

Christina Plainaki[12], Stefano Massetti[3], Xianzhe Jia[4], Alessandro Mura[3], Anna Milillo[3], Davide Grassi [3], Giuseppe Sindoni[2], Emiliano D'Aversa [3], Gianrico Filacchione[3]

Abstract

The temporal and spatial variability of the radiation environment around Ganymede has a direct impact on the moon's exosphere which links Jupiter's magnetosphere with the satellite's icy surface. The dynamics of the entry and circulation inside Ganymede's magnetosphere of the Jovian energetic ions, as well as the morphology of their precipitation on the moon's surface determine the variability of the sputtered-water release. For this reason, the so-called planetary space weather conditions around Ganymede can also have a long-term impact on the weathering history of the moon's surface. In this work, we simulate the Jovian energetic ion precipitation to Ganymede's surface for different relative configurations between the moon's magnetic field and Jupiter's plasma sheet using a single-particle Monte-Carlo model driven by the electromagnetic fields from a global MHD model. In particular, we study three science cases characterized by conditions similar to those encountered during the NASA Galileo G2, G8, and G28 flybys of Ganymede (i.e., when the moon was above, inside, and below the centre of Jupiter's plasma sheet). We discuss the differences between the various surface precipitation patterns and the implications in the water sputtering rate. The results of this preliminary analysis are relevant to ESA's JUICE mission and in particular to the planning and optimization of future observation strategies for studying Ganymede's environment.

[1] Corresponding author christina.plainaki@asi.it
[2] Agenzia Spaziale Italiana –ASI, Via del Politecnico, 00133, Rome, Italy
[3] INAF-IAPS, Via del Fosso del Cavaliere 100, 00133, Rome, Italy
[4] Department of Climate and Space Sciences and Engineering, University of Michigan, Ann Arbor, MI 48109-2143, USA

1. INTRODUCTION AND MOTIVATION FOR THE CURRENT WORK

Jupiter's moon Ganymede is the only natural satellite in the Solar System with an intrinsic magnetic field (Kivelson et al. 1996, 1997; Gurnett et al. 1996). At Ganymede's orbital distance (~15 R_J, with R_J being Jupiter's radius), the Jovian magnetospheric plasma confined by the planet's magnetic field subcorotates with Jupiter at a velocity of ~ 150 km/s (Williams 2001; Kivelson et al. 2004; Bagenal et al. 2016), overtaking the moon which moves with an orbital velocity of ~11 km/s (both velocities have anticlockwise direction, as seen from the North). The magnetic field of Ganymede partially shields the surface from ion impacts, especially at equatorial latitudes (e.g.: Kivelson et al. 1997). The dynamics of plasma entry and circulation inside Ganymede's magnetosphere as well as the properties of the ion precipitation to the surface, are primarily controlled by the reconnection between Jupiter's and Ganymede's magnetic fields (Jia et al. 2010a). With magnetic axis tilted by ~10 degrees with respect to its rotational axis, Jupiter's Plasma Sheet (JPS), which is confined by the magnetic field, oscillates up and down at the satellite's orbit (Kivelson et al. 1998; McGrath et al. 2013), resulting in a dynamic configuration of the circulation and surface precipitation patterns of the different ion populations. The energetic component of the Jovian magnetospheric population is characterized by H^+, O^{n+} and S^{n+} ions (Cooper et al. 2001; Mauk et al. 2004), as evidenced by the NASA Galileo Energetic Particle Detector (EPD) observations, able to detect ions in the 20 keV – 55 MeV energy range (Williams et al. 1992; Paranicas et al. 1999; Mauk et al. 2004).

Past work on modeling Ganymede's ion environment has revealed that the bulk population of Jupiter's plasma enters the moon's magnetosphere mainly through the cusps and at low latitudes in the plasma wake hemisphere (that is, the leading hemisphere), most likely through tail magnetic reconnection (e.g., Williams et al. 1997; Poppe et al. 2018). The maximum ion precipitation to the surface is expected to take place near the Open-Closed magnetic Field lines Boundary (OCFB) regions (e.g.: Kivelson et al. 1997; Plainaki et al. 2015; Fatemi et al. 2016). Energetic ion fluxes (mainly Hydrogen, and multiply charged Oxygen and Sulfur ions) can actually activate complex processes, such as sputtering and radiolysis, releasing H_2O, O_2, H_2, as well as H, O, and OH particles (Johnson 1990; Marconi 2007; Plainaki et al. 2015; Leblanc et al. 2017). At Ganymede, as also at Europa, direct sputtering of surface water molecules, together with water sublimation and radiolysis (leading mainly to O_2 and H_2 release), are believed to generate a tenuous atmospheric envelope around the moon, often referred to as an "exosphere" (e.g.: Plainaki et al. 2015; 2018). Observations by the Plasma Science (PLS; Frank et al. 1997; Collinson et al. 2018) and Plasma Wave Science (PWS; Eviatar et al. 2001) instruments on board the Galileo spacecraft, revealed the existence also of an

ionosphere at Ganymede (Carnielli et al. 2019), consistent with the findings of the Galileo radio occultation experiment (Kliore 1998). Figure 1 shows the complex source and loss mechanisms for the exosphere of Ganymede, coupling the moon's space environment with the Jovian magnetosphere.

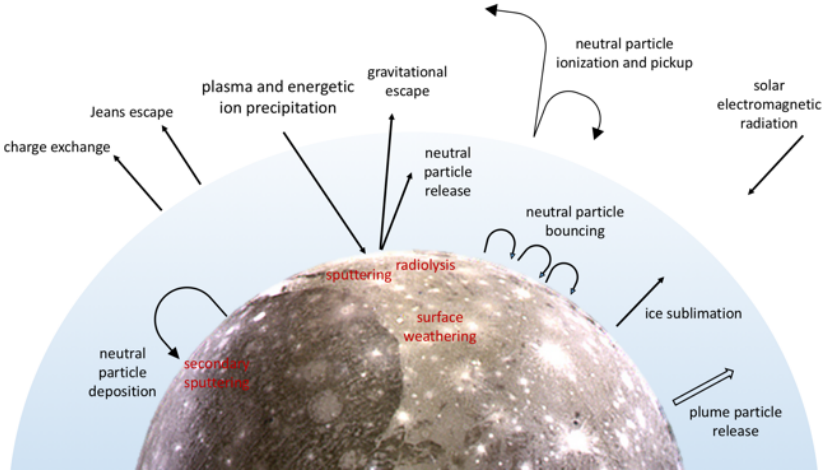

Figure 1: Source and loss mechanisms for the exosphere of Ganymede. The moon's environment is strongly coupled with the Jovian magnetosphere through a series of dynamical processes that contribute to the overall energy exchange between the two systems. Ganymede image credit: NASA/JPL/DLR.

Recent efforts based both on data of past missions (e.g., NASA Galileo) and modeling techniques have been focused on the study of the ion precipitation to Ganymede's surface. Plainaki et al. (2015) performed single-particle Monte Carlo (MC) simulations of the circulation and precipitation to Ganymede's surface of Jovian energetic ions, using electric and magnetic fields from the magnetohydrodynamic (MHD) models of Jia et al. (2008) and Jia et al. (2009). The results presented by these authors corresponded to magnetic and electric field conditions similar to those during the G8 flyby of Galileo and referred only to singly charged Oxygen, Sulfur and Hydrogen ions in the energy range from 1 to 100 keV. The generated ion precipitation maps showed the existence of a shielded region close to the trailing hemisphere surface (at distances smaller than ~1.5 R_G from the moon's centre) and enhancements in the ion flux at near-surface altitudes above the low latitude leading hemisphere (Plainaki et al. 2015; 2020), a result that was further confirmed by other studies as well (e.g.: Fatemi et al. 2016; Poppe et al. 2018; Carnielli et al. 2020). The trajectories of the higher energy ions were shown to be less affected by Ganymede's magnetic field. We note that in the numerical simulations by Plainaki et al. (2015), a "full ion mirroring" condition was included in the code, allowing the ions to be reflected back from both the top and bottom sides of the simulation box.

The three-dimensional self-consistent hybrid model by Fatemi et al. (2016) examined the kinetic

effects of the Jovian plasma interaction with Ganymede's magnetosphere. The model succeeded in capturing both Hall-related and finite-Larmor radius effects in the ion circulation within Ganymede's magnetosphere through the inclusion of the Hall term, although a higher spatial resolution would allow to reveal more detailed features (Dorelli et al. 2015; Tóth et al. 2016; Zhou et al. 2019). The simulations by Fatemi et al. (2016) were based on parameter values given by Jia et al. (2008). The model results reproduced well the Galileo magnetometer measurements taken during each one of the six Galileo flybys. Fatemi et al. (2016) estimated also the precipitating flux of H^+, O^{++}, and S^{+++} ions with energies between 1 and 10^4 keV applying a forward tracing technique using the modelled field values. Their results showed that ions precipitate predominantly at the moon's polar cap region along open fields lines. Moreover, the ion precipitation maps in Fatemi et al. (2016) were in good agreement with Ganymede's surface brightness map by Khurana et al. (2007). We note that the results on ion precipitation presented by Fatemi et al. (2016) corresponded to conditions similar to those during the G8 flyby. The work on the ion precipitation maps by Fatemi et al. (2016) was further extended by Poppe et al. (2018) who used the combination of electric and magnetic fields derived from the hybrid simulations of Ganymede's magnetosphere by Fatemi et al. (2016) and a backwards Liouville tracing technique (e.g., Cooper et al. 2001; Allioux et al. 2013) to quantify the dynamics of thermal and energetic ions near Ganymede. The model of these authors confirmed previous results on the existence of a shielded equatorial region on Ganymede's trailing hemisphere and a non-negligible ion precipitation in the low latitude leading hemisphere. The simulation method used in the work by Poppe et al. (2018) did not utilize a mirroring assumption for the ions exiting the simulation box and they were focused on field conditions at Ganymede representative of the Galileo G8 flyby. Leblanc et al (2017) studied the generation mechanisms and evolution of Ganymede's neutral environment taking into account also the gravitational influence by Jupiter. Their Monte Carlo model followed the dynamical evolution of the exosphere as Ganymede orbits Jupiter, assuming that Jovian ions precipitate to the surface within the open field line regions and considering the OCFB as derived by the auroral observations described in McGrath et al. (2013). Although in the model by Leblanc et al. sputtering and radiolysis were considered among the source mechanisms for the exosphere generation, no variation of the precipitating flux with respect to JPS was considered.

In this paper, for the first time, we perform energetic ion trajectory computations for three distinct configurations between Ganymede's magnetic field and JPS, characterized by magnetic and electric field conditions similar to those during G2, G8, and G28 flyby of Galileo (i.e., the moon above, inside, below the centre of JPS). For each one of the aforementioned configurations we estimate the ion precipitation to the surface for different ion species (H^+, O^{++}, and S^{+++}) in a total energy range from 1

keV to 3 MeV, assuming the energy spectra retrieved by Paranicas et al. (1999). We note that simulating the circulation of the highly charged component of Jupiter's magnetosphere near Ganymede is very important since the energetic ionic environment is believed to be dominated mainly by a combination of H^+, O^{++}, and S^{+++} (Collier and Hamilton, 1995; Keppler and Krupp, 1996; Mauk et al. 2004). The thermal ion population provides no significant contribution to the flux precipitating in the upstream hemisphere of Ganymede (Poppe et al. 2018), whereas the energetic ion flux precipitating to the moon controls surface weathering (e.g., Johnson, 1990; Shi et al. 1995; Hansen and McCord, 2004; Khurana et al. 2007), as well as the production of radiolytic species in the upper surface layers (e.g., Cooper et al. 2001; Gomis et al. 2004; Teolis et al. 2017) and sputtering (e.g., Hall et al. 1998; Marconi, 2007; Turc et al. 2014; Plainaki et al. 2015). Moreover, to estimate the energy exchange between the Jovian magnetosphere and Ganymede, the estimation of the energetic ion precipitation rate over the entire surface is necessary. To this end, and also to globally understand the properties of the exospheric environment, we need to get an in-depth view of the role of the energetic ion environment in provoking direct release of surface particles or/and in activating chemical reactions that lead to particle emissions. The short- or long-term interaction of Jovian ions with the icy surface not only depends on the characteristics of the surface itself (composition, ice state, temperature) but also on the exact way – in terms of impinging flux spatial distribution – the moon gets bombarded by the JPS environment (planetary space weather; Plainaki et al. 2016, 2018, 2020). In this view, in the current paper we focus on the study of the surface precipitation of the Jovian energetic ion population. The paper is organized as follows. In Section 2, we describe the model of ion circulation within Ganymede's magnetosphere. The results of the simulations are presented in Section 3, whereas in Section 4 we analyse the differences between the various ion precipitation patterns corresponding to different configurations of Ganymede's field with respect to the JPS, and we discuss the implications in Ganymede's exosphere generation and surface weathering history, from a planetary space weather perspective.

2. MODEL DESCRIPTION

To obtain the spatial distribution of the energetic ion circulation around Ganymede and to map their precipitation to the surface, we apply a single-particle Monte Carlo model based on the technique proposed previously by Plainaki et al. (2015) assuming a background magnetic field configuration. In particular, we assume the magnetic and electric field data derived from the Jia et al. (2008) and Jia et al. (2009) global MHD model of Ganymede's magnetosphere, which has been shown to reproduce with high fidelity the magnetic field and plasma measurements during multiple Galileo flybys of

Ganymede. We assume that the energetic component of the Jovian magnetospheric population is characterized by H^+, O^{n+} and S^{n+} ions (Cooper et al. 2001; Mauk et al. 2004).

We trace the trajectories of Jovian ions of different species for the full three-dimensional ion velocity distribution. In addition to the simulations performed in Plainaki et al. (2015), in the current paper we calculate the trajectories of multiply charged ions (e.g., O^{++}, S^{+++}) at discrete energies covering the range from 1 to 3000 keV. In our simulations, the standard ''GphiO" coordinate system is used: X is along Ganymede orbital motion (and the JPS flow direction, too), Z is along the Jupiter's spin axis, and Y points toward Jupiter. The $\pm10 \times \pm10 \times \pm10$ R_G simulation box is centred to the moon (with R_G = 2,634 km being the Ganymede's radius), with a spatial resolution of 0.1 R_G , for a total of 8×10^6 cells. In each run, 2×10^6 test particles are launched with a defined initial energy but random initial direction: to mimic the ion flow of the JPS, which co-rotates with Jupiter faster than Ganymede along its orbit and then overtakes and embeds the moon, we place a 1 R_G thick planar "source surface" perpendicular to the moon's orbit, located between X = -3 R_G and X = -4 R_G upstream of Ganymede (the stand-off distance of the magnetopause is ~2 R_G). The particle tracking is achieved via the Boris-Buneman Lorentz force integrator (Boris 1970) over the gridded magnetic and electric field data output from the published MHD simulations, which is interpolated within each cell. Weighted physical quantities associated with each moving test particle are stored into a 200×200×200×6 array, resulting in a 3D distribution of density, energy, velocity Cartesian components, and **V** parallel to **B** component. Test particles ending their paths by hitting the body surface populate a 180×360 array, resulting in a latitude per longitude distribution of ion impacts, energy and flux. To achieve an as much as possible realistic simulation, we have to prevent the artificial "loss" of particles due to both the compression of the magnetic field lines on the trailing side of Ganymede and the finite size of the simulation box. As a workaround, we include in the code a "full mirroring" condition, as in Plainaki et al. (2015). This simply means that the test particles crossing the Z = $\pm10R_G$ planes are reflected back from both the top and bottom sides of the simulation box. It must be noted that allowing the ions to freely escape the simulation box along the open magnetic field line (connected to Jupiter) would lead to an underestimation of the ion circulation and the ion precipitation into the polar caps, which would not be compatible with current knowledge. Since Ganymede is embedded within the JPS, about 3 $R_J \cong 80$ R_G thick at its orbit (Kivelson et al. 2004), ions are expected to (re)enter in the simulation box, bouncing back somewhere along the field lines connected to Jupiter, or spreading in from the contiguous region of the JPS. Because of our "full mirroring" assumption, the results in this work have to be considered as upper limits for the ion circulation around Ganymede, and interpreted consequently.

In this paper, for the first time, we perform ion trajectory computations for three sets of MHD simulation data corresponding to three different configurations of Ganymede's magnetic field with respect to JPS, characterized by magnetic and electric field conditions similar to those during the G2 (science case (i)), G8 (science case (ii)), and G28 (science case (iii)) flybys of Galileo. The trajectories during the Galileo G2, G8, and G28 flybys of Ganymede are discussed in Jia et al. (2010). We define, accordingly, the following science cases:

- science case (i): Ganymede is above the centre of JPS
- science case (ii): Ganymede is close to the centre of JPS
- science case (iii): Ganymede is below the centre of JPS

For each one of the aforementioned science cases, we run simulations for H^+, O^{++}, and S^{+++}, at the discrete energies of 1, 5, 10, 30, 50, 100, 300, and 3000 keV. To normalize the simulation results and get the absolute flux of ions precipitating to the surface (in $cm^{-2}\ s^{-1}\ keV^{-1}$), we insert in our code the species-specific distributions as determined by Paranicas et al. (1999) from Galileo/EPD data. We considered an additional 1:5 scaling of the fluxes above/below the centre of JPS (science case (i) and (iii), respectively) with respect to the ones near the centre of JPS (science case (ii)), to take into account the relative densities at the orbit of Ganymede, as reported in Kivelson (2004).

3. RESULTS

Figure 2 presents snapshots in the XY, XZ, and YZ planes of the H^+ flux at initial energy equal to 10 keV, for the three considered science cases. The ion circulation and surface precipitation patterns in Figure 2 are compatible with a flow mainly through the cusps and the polar caps, guided strongly by the position of the OCFB. A relatively smaller contribution in the low-latitude surface precipitation at the leading side comes from the ions drifting around the moon, populating the magnetotail. The surface precipitation of H^+ is in general asymmetric both with respect to the leading/trailing and Jupiter/anti-Jupiter facing sides of Ganymede's surface. In all three science cases, the surface precipitation of H^+ takes place at higher latitudes at the trailing side with respect to the leading one (see panels (b), (e), and (h) in Figure 2).

The presence of Alfvén wings that bend the open magnetic field lines above Ganymede's polar caps is evident in Figure 2. Their form is different for the three considered science cases. Comparing science cases (i) and (iii), we note that the form and the position of the Alfvén wings are not perfectly anti-asymmetric (see also Jia et al. 2008). In particular, as shown in panels (b) and (h), the Alfvén wings are significantly wider and more elongated in science case (iii). In general, the H^+ flux

decreases considerably inside Ganymede's magnetosphere, especially in the upstream region shielded by the closed magnetic field lines (see, for instance, Figure 2, panels (b), (e), and (h)). However, the flux inside the Alfvén wings appears relatively increased if compared to the one above the low latitude upstream hemisphere; regions of lower ion intensity, nevertheless, appear there also (see panels (c) and (i) in Figure 2). In science case (ii) the relative increase of the H^+ flux inside the Alfvén wings is more intense with respect to the other two cases, a fact that reflects the higher ion densities near the centre of JPS (Kivelson et al. 2004).

As shown in panels (a) and (g) of Figure 2 (XY plane snapshots corresponding to science cases (i) and (iii), respectively) and also in panels (c) and (i) (YZ plane snapshots corresponding to science cases (i) and (iii), respectively), there is a significant asymmetry between the Jupiter and the anti-Jupiter facing sides in the H^+ precipitation to high-latitude/polar caps surface regions. Such an asymmetry is in the opposite sense for science cases (i) and (iii) and for the Northern and Southern hemispheres. In particular, in science case (i), the high latitude/polar cap surface of the anti-Jupiter facing side of the Northern hemisphere receives slightly more intense H^+ fluxes than the opposite side (see panels (a) and (c) in Figure 2). In science case (iii), instead, an extended region of the high latitude/polar cap surface of the Jupiter facing side of the Northern hemisphere is bombarded by more intense H^+ fluxes with respect to the opposite side, which is, at large extent, shielded from the magnetospheric particles (see panels (g) and (i) in Figure 2). The reversed situation takes place at the Southern hemisphere; in particular, in science case (i), higher fluxes precipitate at the high latitude/polar cap surface of the Jupiter facing side of the Southern hemisphere (see panel (c) in Figure 2), whereas in science case (iii), higher fluxes precipitate at the high latitude/polar cap surface of the anti-Jupiter facing side of the Southern hemisphere (see panel (i) in Figure 2). In science case (ii) (Ganymede is near the centre of JPS), the asymmetries in the high latitude/polar cap precipitation are attenuated.

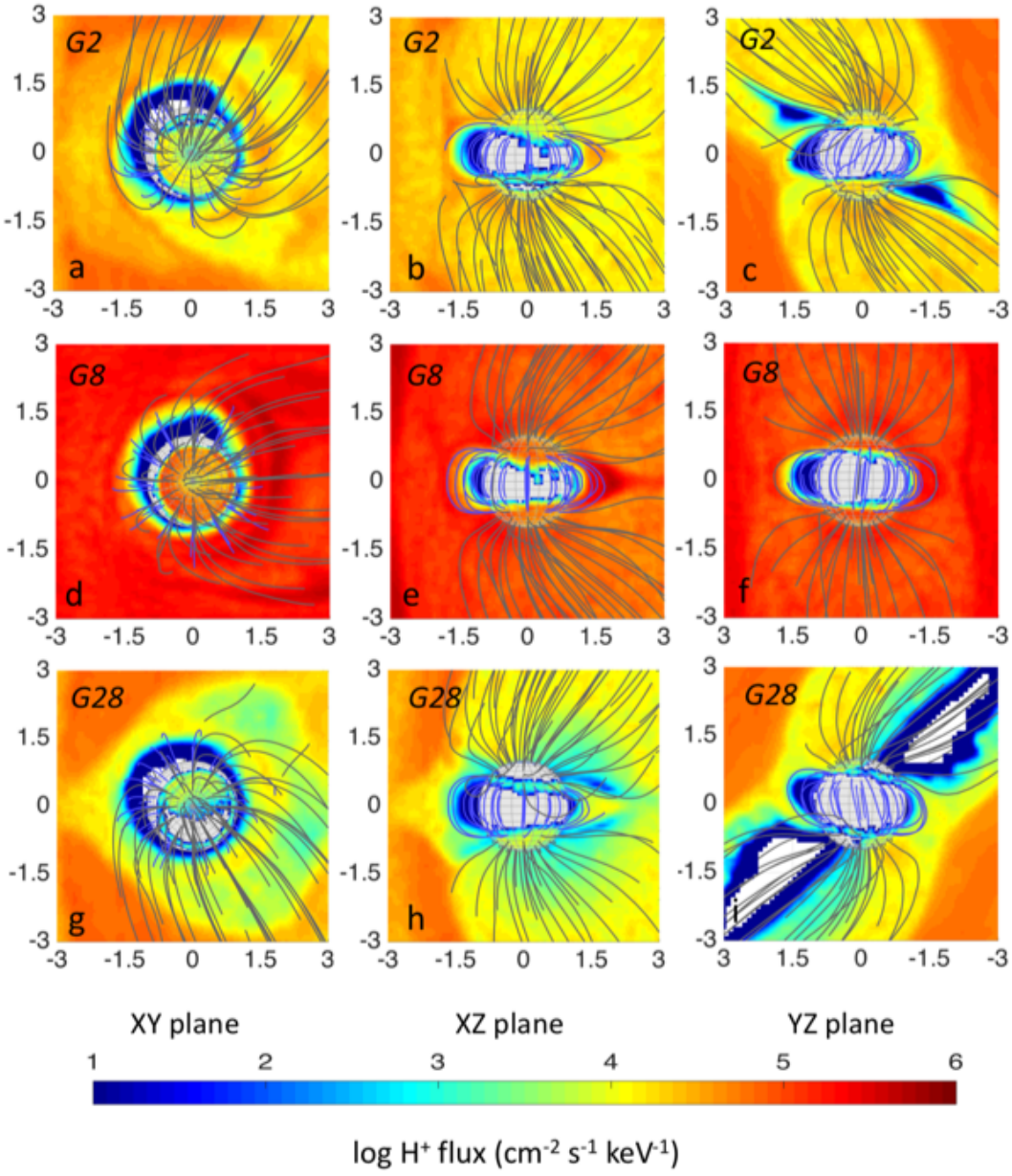

Figure 2: H^+ flux configuration around Ganymede at initial energy equal to 10 keV for three different configurations of the moon's magnetic field with respect to JPS: panels (a), (b), and (c) correspond to science case (i) (Ganymede is above the center of JPS); panels (d), (e), and (f) correspond to science case (ii) (Ganymede is near the center of JPS); panels (g), (h), and (i) correspond to science case (iii) (Ganymede is below the center of JPS). The GPhiO coordinates have been used: X is along the ambient flow direction (and Ganymede's orbital motion), Z is along the Jupiter's spin axis, and Y points toward Jupiter (in units of Ganymede's radii). First column (panels (a), (d), and (g)) shows the XY-, second column (panels (b), (e), and (h)) shows the XZ- and third column (panels (c), (f), and (i)) shows the YZ-projections. White squared areas in panel (i) indicate regions where ion circulation could not be simulated due to the absence of background magnetic field data.

Figure 3 shows the expected H^+ precipitation maps in science case (ii) (Ganymede is near the centre of JPS) for different initial ion energies. The W longitude system has been used meaning the leading hemisphere is at long ~ 90^0 and long ~ 0^0 is at the Jupiter-facing hemisphere apex. For both North and South hemispheres, there is a trailing-leading asymmetry in the H^+ surface precipitation that gets more and more attenuated as the initial ion energy increases (for instance, compare panels (a) and (c) with (d) and (f)).

As seen in both Figure 2 and Figure 3 (which refers to science case (ii)), the H^+ flux diverted around the magnetopause precipitates onto the low-latitude surface of Ganymede guided primarily by the position of the OCFB region. The low latitude/equatorial H^+ circulation (see panels (c), (f), and (i) of Figure 2), for all the considered science cases, show a more intense flux in the anti-Jupiter direction (negative Y axis in Figure 2). This asymmetry is more apparent in science case (ii), especially in the Northern hemisphere. Indeed, Figure 3 shows that the low latitude/equatorial H^+ flux at the anti-Jupiter facing side of the Northern hemisphere (around longitude ~ 180^o) reaches lower latitudes than those at the opposite side (around longitude ~ 0^o), at least for energies up to 100 keV. Also at the Southern hemisphere such a Jupiter/anti-Jupiter asymmetry exists, but it is most evident in the low latitude/equatorial H^+ flux with initial energy up to 10 keV.

Figure 4 provides XZ projections of the O^+ and O^{++} circulation around Ganymede at initial energy equal to 30 keV for the three considered science cases. The presence of Oxygen ions inside the Alfvén wings is caused by two effects: their relatively large rigidity (which is enough to allow ions to partially penetrate), and, at a larger extent, the plasma injection inside the wings (i.e., the mirroring assumption; see Section 2 and Plainaki et al. 2015).

The results presented in Figure 4 confirm that the properties of the surface precipitation of Oxygen ions depend strongly on their actual charge state. Indeed, lower rigidity O^{++} particles (the magnetic rigidity of an ion is defined as the ratio of its momentum to its charge, i.e., $= \frac{mv}{q}$, where m is the ion mass, v its velocity and q its charge) are more strongly guided by the magnetic field than O^+ and they reach the low latitude leading hemisphere with higher fluxes, for all three science cases (see panels (d), (e), and (f) in Figure 4). Equivalently, the surface of the moon's trailing hemisphere (plasma upstream), appears slightly more shielded from O^{++} than from O^+. This applies for our single-particle MC model but in case of ideal MHD models where ion gyromotion is averaged out and the ions and electrons are combined into a single fluid such asymmetries would not be present (see also discussion in Paty et al. 2009).

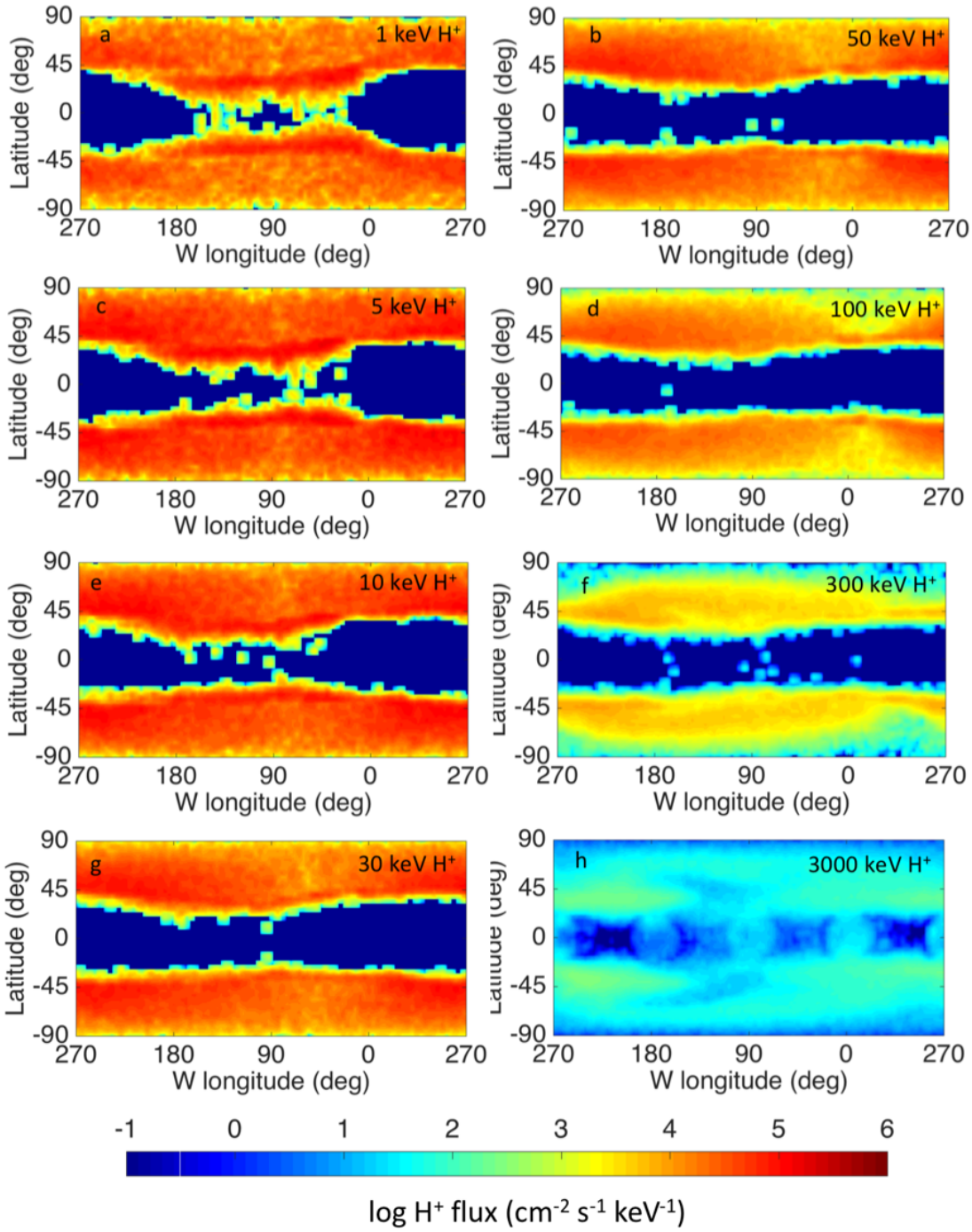

Figure 3: H^+ precipitation maps in science case (ii) (Ganymede is near the centre of JPS) corresponding to different initial energies. The W longitude system has been used meaning the leading hemisphere is at long ~ 90^0 and long ~ 0^0 is at the Jupiter-facing hemisphere apex.

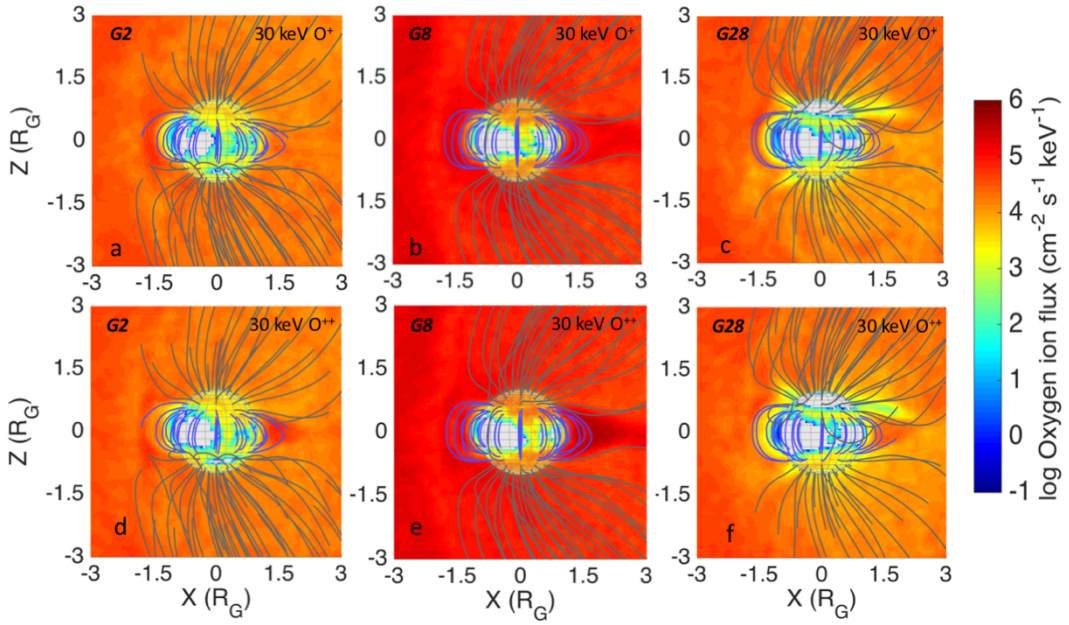

Figure 4: XZ projections of the O^{+} and O^{++} circulation around Ganymede at initial energy equal to 30 keV for three different configurations of the moon's magnetic field with respect to JPS: panels (a) and (d) correspond to science case (i) (Ganymede is above the centre of JPS); panels (b) and (e), correspond to science case (ii) (Ganymede is near the centre of JPS); panels (c) and (f) correspond to science case (iii) (Ganymede is below the centre of JPS). The GPhiO coordinates have been used: X is along the ambient flow direction (and Ganymede's orbital motion), Z is along the Jupiter's spin axis, and Y points toward Jupiter (in units of Ganymede's radii).

The precipitation patterns in Figure 4 are compatible with a flow through the cusps/polar caps and a mounting of the ions in the downstream region. Indeed, as seen in all three panels of Figure 4, the Oxygen ion flow gains access mainly through the OCFB region and at low latitudes of the wake hemisphere, a result that confirms previous simulations by Paty and Winglee (2004), Paty et al. (2008), Plainaki et al. (2015), and Poppe et al. (2018). In the context of comparative planetary space weather science (see, for instance, discussions in Plainaki et al. (2016) and André et al. (2018)), this situation reminds the motion of the ions in the Earth's plasma sheet, in the magnetotail reconnection region (e.g., Chen and Palmadesso, 1986). Our simulations show that ions circulating inside Ganymede's magnetosphere can gain access along the closed field lines back to Ganymede's surface in the leading (plasma wake) hemisphere. Moreover, our results do not exclude the possibility that part of that redirected flow returns back also towards the trailing hemisphere.

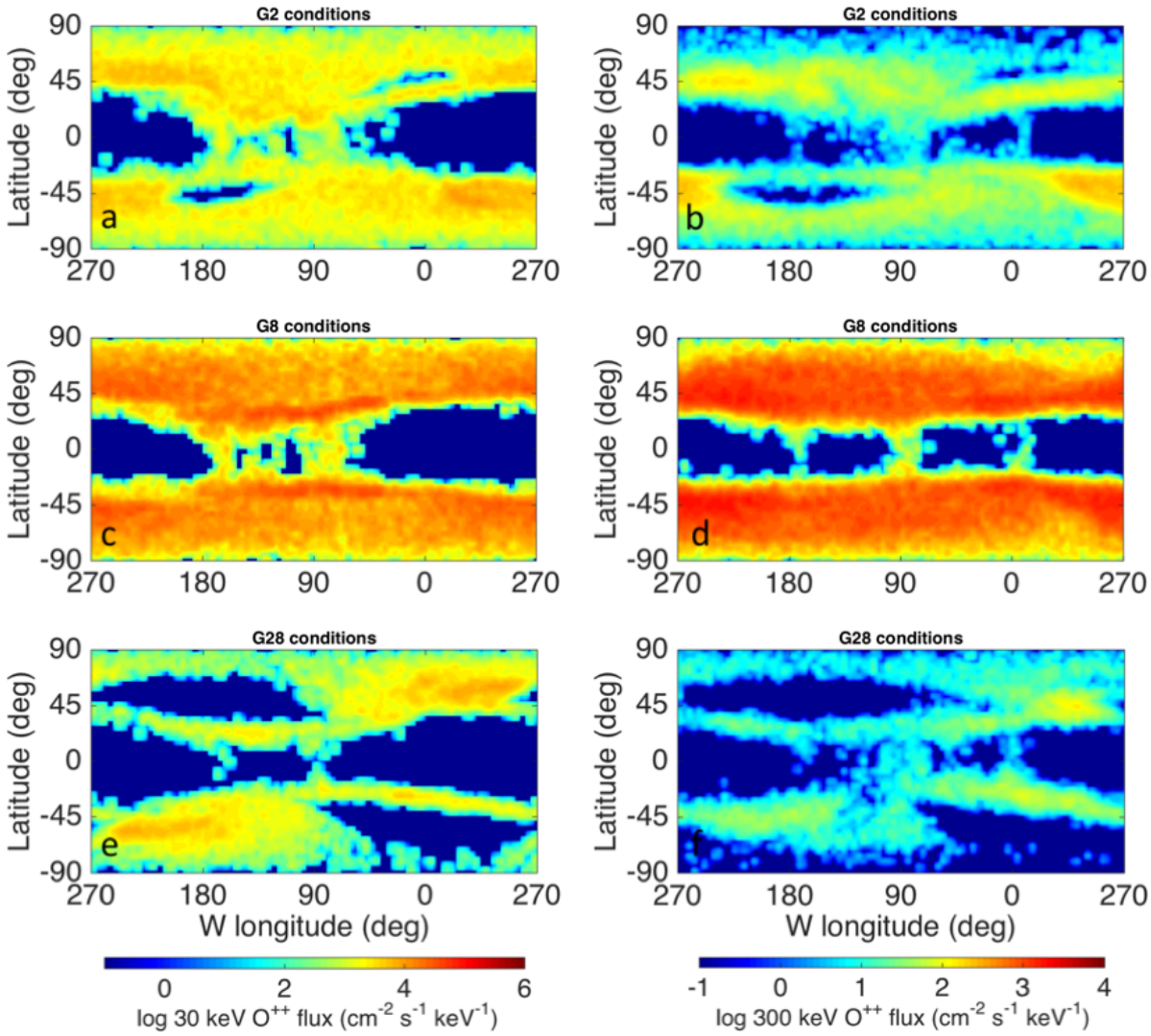

Figure 5: 30 keV O^{++} (panels (a), (c), and (e)) and 300 keV O^{++} (panels (b), (d), and (f)) precipitation to Ganymede's surface for different configurations of the moon's magnetic field with respect to JPS. Panels (a) and (b) correspond to magnetic field conditions similar to those during the Galileo G2 flyby (Ganymede above the centre of JPS), panels (c) and (d) to those during the Galileo G8 flyby (Ganymede near the centre of JPS), panels (e) and (f)) to those during the Galileo G28 flyby (Ganymede below the centre of JPS). The W longitude system has been used meaning the leading hemisphere is at long ~ 90^0 and long ~ 0^0 is at the Jupiter-facing hemisphere apex.

Figure 5 presents the O^{++} precipitation to Ganymede's surface for the three considered configurations of the moon's magnetic field with respect to JPS, for initial ion energies 30 keV and 300 keV. The respective surface precipitation patterns are compatible with a flow guided strongly by the position of the OCFB. The surface precipitation of O^{++} at initial energy equal to 30 keV (Figure 5, panels (a),(c), and (e)) is in general asymmetric both with respect to the leading/trailing and Jupiter/anti-Jupiter facing sides of Ganymede's surface. As in the case of H^+, and even more markedly, for all the

considered science cases, there is a significantly increased flow in the anti-Jupiter low latitude/equatorial surface regions of the leading side of Ganymede (longitude range ~ [90° 180°]; latitude range ~ [-45° 45°]). We note that this seems to apply also for science case (iii) (see panel Figure 5, panel (e)), although the statistics of the simulation do not allow a definite conclusion. In general, such an effect is expected for all types of ions and is due to the ion cyclotron motion and finite Larmor radius effects. Similar results are obtained also for the case of O^{++} at initial energy equal to 300 keV (Figure 5, panels (b), (d), and (f)), however, the aforementioned asymmetries appear somehow attenuated, probably due to the ions' higher magnetic rigidities. We note also that for science case (i), the heavy O^{++} flow at initial energy equal to 30 keV (see Figure 5, panel (a)) has local maxima within the trailing hemisphere, in its Jupiter-facing sector (270°W-360°W) for southern latitudes ~65°S-45°S and in its anti-Jovian sector (180°W-270°W) for Northern latitudes ~40°N-55°N. An almost antisymmetric situation is noted for science case (iii) (see Figure 5, panel (e)): the flow has local maxima within the trailing hemisphere, in its Jupiter-facing sector (270°W-360°W) for northern latitudes ~45°N-65°N and in its anti-Jovian sector (180°W-270°W) for southern latitudes ~45°S-65°S.

In all three science cases, the surface precipitation of the O^{++} flux at initial energies equal to 30 keV and 300 keV takes place at higher latitudes at the trailing side with respect to the leading one. The flow downtail is strongly redirected near the equatorial plane. This result is consistent with simulations performed by Shay and Swisdak (2004), Paty et al. (2009) and Toth et al. (2016). In general, the Oxygen ion flux distribution on the low latitude surface of the leading hemisphere, at both initial energies of 30 keV and 300 keV, is more extended than the one of Hydrogen ions of the same energy (compare, for instance, Figure 5 panels (c) and (d) with Figure 3 panels (g) and (f)).

Figure 6 presents the S^{+++} precipitation to Ganymede's surface for the three considered configurations of the moon's magnetic field with respect to JPS, for initial ion energies equal to 30 keV (panels (a), (c), and (e)) and 300 keV (panels (b), (d), and (f)). As in the case of O^{++}, for all the considered science cases, there is a significantly increased flow in the anti-Jupiter low latitude/ equatorial surface regions of the leading hemisphere.

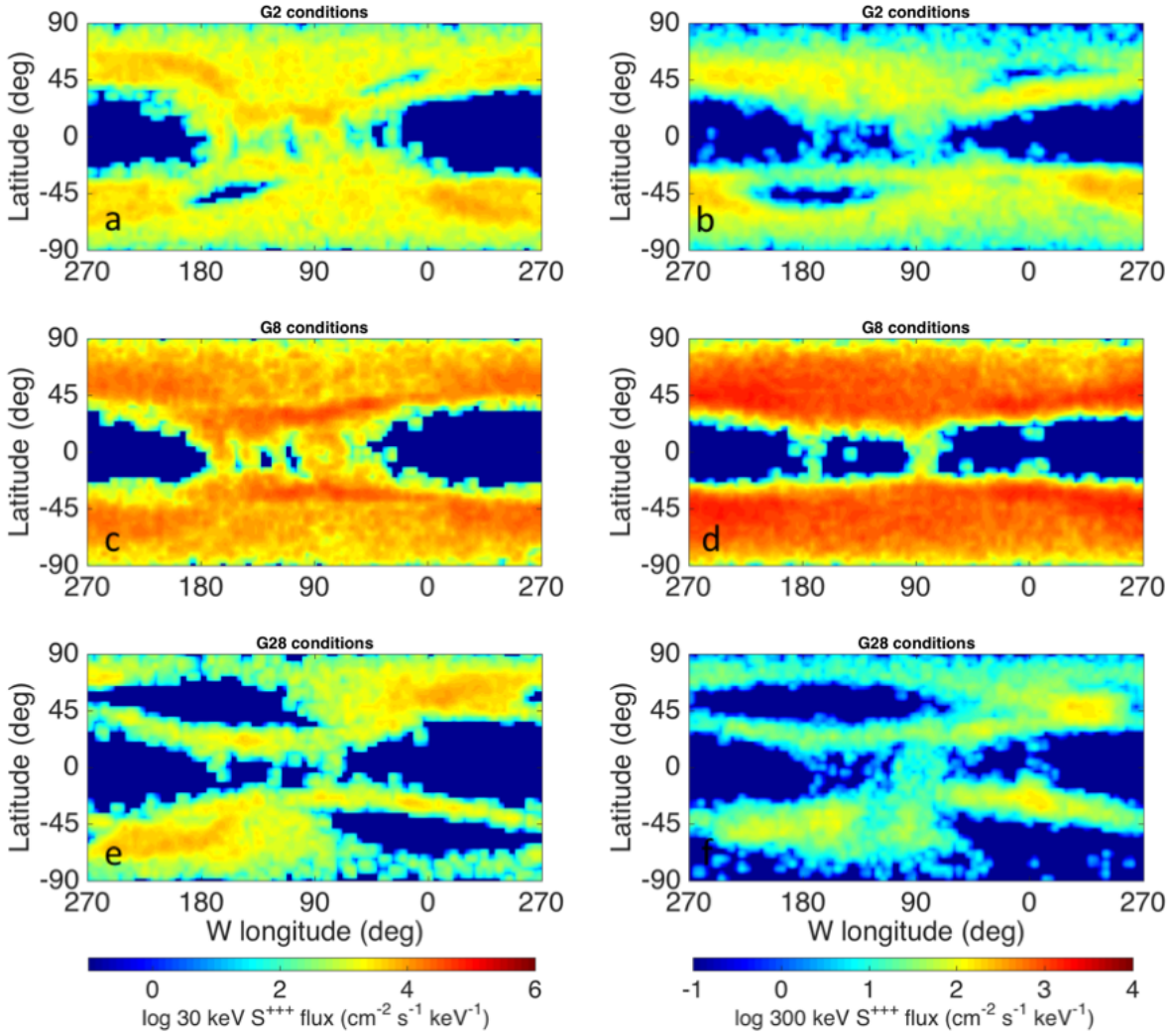

Figure 6: 30 keV S^{+++} (panels (a), (c), and (e)) and 300 keV S^{+++} (panels (b), (d), and (f)) precipitation to Ganymede's surface for different configurations of the moon's magnetic field with respect to JPS. Panels (a) and (b) correspond to magnetic field conditions similar to those during the Galileo G2 flyby (Ganymede above the centre of JPS), panels (c) and (d) to those during the Galileo G8 flyby (Ganymede near the centre of JPS), panels (e) and (f)) to those during the Galileo G28 flyby (Ganymede below the centre of JPS). The W longitude system has been used meaning the leading hemisphere is at long ~ 90^0 and long ~ 0^0 is at the Jupiter-facing hemisphere apex.

In conclusion, the majority of the H^+ impacts occur in the polar regions, due to their relatively low magnetic rigidity which limits their capacity to penetrate in the closed field lines region. O^{++} and S^{+++} due to their higher magnetic rigidity reach lower latitude surface regions in the plasma downstream hemisphere, nevertheless, the main flux is still concentrated near the OCFB region. The asymmetries in the precipitating flux are attenuated as a function of both the particle rigidity and the configuration of Ganymede's magnetic field with respect to JPS.

394 4. DISCUSSION

395

396 The results of the simulations performed in the context of the current study evidence a series of
397 notable features in Ganymede's magnetosphere and reveal, for the first time, some important aspects
398 of the variability of the ion-moon interactions, in terms of surface bombardment patterns. The results
399 considering the case of Ganymede being near the centre of Jupiter's plasma sheet are qualitatively
400 similar to those of other works where different methodological approaches have been followed (e.g.,
401 Fatemi et al. (2016); Poppe et al. (2018)), nevertheless, some quantitative differences are existent.
402 Below we discuss some of the main findings of the current work also through a comparison (where
403 possible) with the results of past efforts.

404

405 4.1. Confirmation of previous findings and main add-ons

406

407 The results of the current study, for all the considered configurations between Ganymede's magnetic
408 field and JPS, confirm that the ion circulation above the moon's polar caps is strongly determined by
409 the exact form of the Alfvén wings. Our particle trajectory simulations show that the Alfvén wings
410 when Ganymede is above and below the centre of the JPS are not perfectly anti-asymmetric. This
411 happens because the magnetic field in the Jupiter and anti-Jupiter facing sides is asymmetric (Jia et
412 al. 2008).

413

414 Regions of lower or no flux inside the Alfvén wings are evident in the H^+ ion circulation maps in both
415 science cases (i) and (iii) (see Figure 2, panels (c) and (i)) and also in the heavier ion circulation maps.
416 Figure 7 shows the circulation maps of O^{++} at initial energy equal to 30 keV in science cases (i) and
417 (iii). It is evident that cavities within the Alfvén wings depend both on the ion magnetic rigidity and
418 the configuration of the moon's magnetic field with respect to JPS. Plasma cavities within the Alfvén
419 wings have been also found in the simulations by Toth et al. (2016) but not in the simulations by
420 Fatemi et al. (2016).

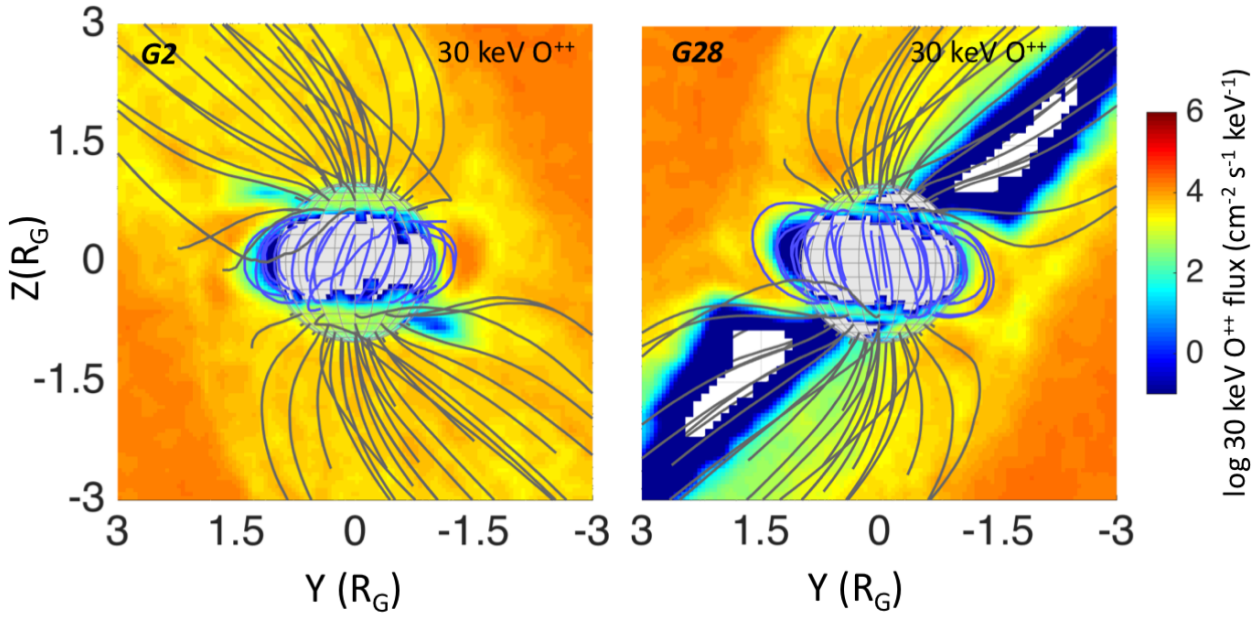

Figure 7: Circulation maps of O^{++} at initial energy equal to 30 keV in science case (i) (Ganymede above the centre of JPS; left panel) and (iii) (Ganymede below the centre of JPS; right panel). The GPhiO coordinates have been used: X is along the ambient flow direction (and Ganymede's orbital motion), Z is along the Jupiter's spin axis, and Y points toward Jupiter (in units of Ganymede's radii).

The surface precipitation patterns for all three energetic ion species considered in this study show a large-scale dichotomy in surface fluxes between the polar and the lower latitude regions of Ganymede. In particular, longitudinal variations in the width of the equatorial shielded region are observed between the precipitation maps of the three ion populations, with the widest latitudinal shielding occurring on the trailing hemisphere (plasma upstream) for ions with low initial rigidity (e.g., H^+) in science case (iii). The shielding of the equatorial region of the leading hemisphere depends not only on the initial ion rigidity but, possibly, also on the ion motion in the magnetotail towards the downstream surface.

In this work, we find that the magnetospheric ion fluxes are accelerated mainly towards the surface at the OCFB regions of both the trailing and leading hemispheres and in the magnetotail. The ion fluxes integrated in energy (in cm^{-2} s^{-1}) precipitating to Ganymede's surface according to the simulation results of this work are presented in Table 1. The total ion precipitating rate on Ganymede's surface (in s^{-1}), for each science case and ion species is given in Table 2. We note that the higher flux/rate corresponds to H^+ ions when Ganymede's magnetic field is near the centre of JPS. The exact morphology of the ion precipitation patterns at the leading hemisphere depends on the configuration of Ganymede's magnetic field with respect to JPS. The simulations of the current work

444 confirm qualitatively our past findings in Plainaki et al. (2015) which however referred only to
445 science case (ii) and considered a limited range of ion initial energies (1-100 keV). The current work,
446 in addition, integrates our previous effort by considering three different configurations of the
447 magnetic field plus a wide range of ion energies, including multiply charged heavy ions. Current
448 simulations show that there is a longitudinal asymmetry between the ion precipitation in the low-
449 latitude trailing and leading hemispheres, not only when Ganymede is near the centre of JPS (see
450 works by Poppe et al. (2018), Fatemi et al. (2016)), but also when it is above or below it.
451
452 Figure 8 shows the low energy H^+ precipitation maps in science case (i) (panels (a) and (c)) and
453 science case (iii) (panels (b) and (d). In science cases (i) and (iii), Hydrogen ions with initial energy
454 1 and 5 keV almost do not reach some higher-latitude regions of the surface (see Figure 8, regions
455 within the dashed circles). The existence of these "shielded areas" is due to the geometry of the
456 electromagnetic fields, which being tilted with respect to Ganymede's rotation axis create specific
457 access paths for the impinging populations. For each ion population of a specific magnetic rigidity,
458 the form and position of these "shielded areas" is different, depending on the orientation of
459 Ganymede's magnetic field with respect to JPS. Indeed, this effect is also evident in the heavy ion
460 populations (see, for instance, panels (a) and (e) of Figure 5 and panels (a) and (e) of Figure 6).
461
462 Our results considering science case (ii) are in agreement with the findings of other studies based
463 either on hybrid simulations of Ganymede's magnetosphere (e.g.: Fatemi et al. 2016) or single
464 particle models using either a self-consistent plasma model (e.g.: Poppe et al. 2018) or a superposition
465 of Ganymede and Jovian magnetic fields as background fields (Allioux et al. 2013). In particular, the
466 current study shows that in science case (ii) most of the O^{++} and S^{+++} low-latitude/equatorial flux
467 precipitates on the anti-Jupiter-facing side of Ganymede's leading hemisphere, in agreement with
468 results by Poppe et al. (2018). For the same science case (ii), we find that no low-energy ($E < 30$ keV)
469 ion fluxes have access to Ganymede's low latitude ($< 20^0$) trailing hemisphere, in agreement with
470 both Poppe et al. (2018) and Allioux et al. (2013), whereas they can impact the equatorial regions of
471 the leading side. Protons with energies in the 30 keV–300 keV range almost cannot reach Ganymede's
472 surface in the equatorial regions of both the leading and trailing sides, in agreement with Poppe et al.
473 (2018). We note that the results by Allioux et al. (2013) for 25 keV, 300 keV, and 6 MeV H^+ and O^{++}
474 densities in the near-Ganymede space display local depletions also over the polar regions of
475 Ganymede and near the "cusp" regions where the total fields reach a minimum in the simple
476 superposition model of magnetic fields. Such a result may be due to the non-simulation of ion
477 bouncing between Ganymede's poles and Jupiter, similar to the non-mirroring case examined in

Plainaki et al. (2015) (see their Fig. 2). In any case, the results of Allioux et al. (2013) show a general decrease in ion density as the ion energy increases and this is qualitatively in agreement with the results of the current paper.

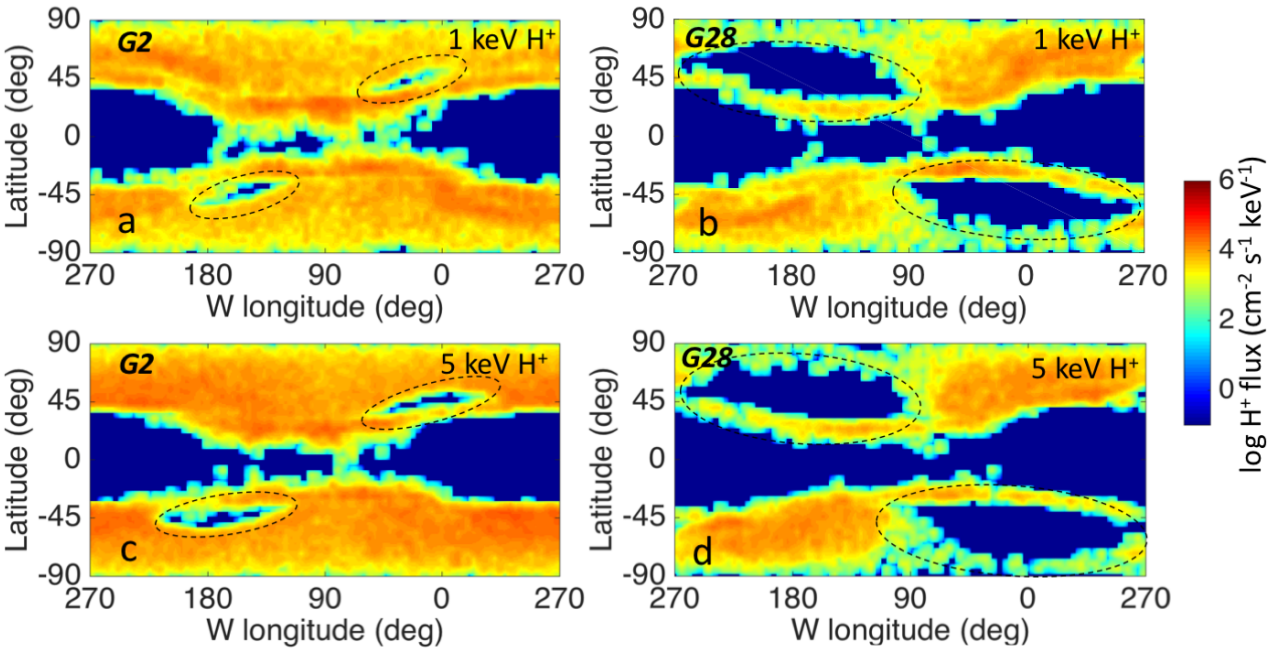

Figure 8: Low energy H^+ precipitation maps in science case (i) (panels (a) and (c)) and science case (iii) (panels (b) and (d). The regions indicated inside the dashed-line circles are regions with low or zero precipitating flux defined here as "shielded areas". For each ion population of a specific magnetic rigidity, the form and position of the "shielded areas" depends on the orientation of Ganymede's magnetic field with respect to JPS. The W longitude system has been used meaning the leading hemisphere is at long ~ 90^0 and long ~ 0^0 is at the Jupiter-facing hemisphere apex.

4.2. The importance of studying the energetic H^+ circulation

H^+ is the most abundant species in the near-Ganymede environment in the non-thermal energy range (i.e., above a few keV; see Poppe et al. (2018)). Understanding the properties of energetic Hydrogen ions is of particular importance when studying the interactions of the surface/exosphere system of Ganymede with the Jovian magnetosphere, also in the context of planetary space weather within the giant planetary system. In particular, the distribution of H^+ (with an initial energy of 10 keV; see Figure 2) can be considered as a good means of studying the influence of Ganymede's intrinsic magnetic field in the ion flux distribution in the near-surface environment. This is because the motion of these ions is driven by the magnetic field in a more significant way than the heavier JPS ions, even when the latter ones are multiply charged (e.g., O^{++} or S^{+++}). This is due to the lower magnetic rigidity

of H^+; in particular, the magnetic rigidity of H^+ is half of the rigidity of O^{++} under the same energy and therefore small-scale variations in the H^+ distributions should be in general more evident. We note that this applies for our single-particle Monte Carlo model whereas in case of ideal MHD models, where ion cyclotron motion is averaged out and the ions and electrons are combined into a single fluid, such a difference between the circulation of light and heavy ions would not be present. Also in the context of possible future planetary space weather measurements (e.g., with JUICE), being H^+ of low magnetic rigidity, the detection of its distribution in the near-Ganymede space would allow us to sense the short-term variability of the interactions between JPS and the moon itself. Indeed, such a measurement together with ENA imaging can provide a dynamic picture of Ganymede's magnetosphere, also as a function of the external to the moon conditions.

The total H^+ precipitation rate when Ganymede is near the centre of JPS (science case (ii)) is estimated to be 4.7×10^{24} s^{-1} whereas the maximum H^+ flux is estimated to be $\sim2.5\times10^{7}$ cm^{-2} s^{-1}. This value is somehow higher than the one estimated by Poppe et al. for the energetic H^+ population above the polar cap (8.4×10^{6} cm^{-2} s^{-1}). This difference may be due to small differences in the energetic ion spectra used in the two works and/or to specific assumptions and modeling techniques. Indeed, since Poppe et al. (2018) assumed no ions being reflected back into the domain, their estimates may be considered as a lower bound and current results can serve as the upper bound. The energy spectrum by Paranicas et al. (1999) considered in the current work refers to H^+ energies bigger than 1 keV whereas the energy spectrum by Mauk et al. (2004) to H^+ energies bigger than 10 keV). Of course, our "full-mirroring" assumption leads probably to a relative overestimation of the flux precipitation on the polar surface, nevertheless, a non-mirroring assumption would lead to unrealistic situations as demonstrated in Plainaki et al. (2015).

The results of this study show that the H^+ flux with initial energy of 10 keV is diverted by Ganymede's magnetic field at the distance of ~ 1.8-2 R_G from the moon's centre in science cases (i) and (iii), whereas in science case (ii) the flux is depleted at a closer to the surface distance (i.e., at about 1.4 R_G from the surface; see Figure 2 panels (b), (e), and (g)). The width of the upstream magnetosphere in the simulations by Fatemi et al. (2016), who applied a three-dimensional self-consistent hybrid model of plasma where ions are treated as particles and electrons are considered as massless charge-neutralizing fluid, is somehow broader. Such a difference may be attributed to the omission of energetic particles in the model of these authors, whereas the MHD models by Jia et al. (2008, 2009), from which the electromagnetic fields were extracted for our simulations, included the contribution

533 of energetic particles to the total pressure in their model in order to obtain a simulated magnetosphere
534 whose size is consistent with observations.
535
536 Our simulations also show enhanced Hydrogen ion flows above the polar caps for all the considered
537 science cases. Such a result confirms previous outcomes of hybrid simulations by Fatemi et al. (2016)
538 corresponding to the G8 (Ganymede near the centre of the JPS) flyby of Galileo. In this paper, in
539 addition, we present a new result: the ion precipitation on Ganymede's polar cap is more extended
540 when Ganymede is above the centre of JPS than when it is below. In reality, the entire precipitation
541 patterns are different in these two cases, not only for H^+ but also for the heavy ions (see, for example,
542 Figures 5 and 6). The total H^+ precipitation rate, however, is maximum in science case (ii) (see also
543 Table 2).
544
545 4.3. Heavy ions
546
547 Both energetic O^{++} and S^{+++} can penetrate Ganymede's magnetosphere down to the surface within the
548 equatorial, closed field line region (i.e., at latitudes less than $\pm 30^{\circ}$). Additionally, especially for
549 science cases (i) and (ii) the flux of energetic O^{++} and S^{+++} to Ganymede's equatorial region shows
550 local increases on the anti-Jupiter facing leading hemisphere. This shift of the maximum equatorial
551 precipitation away from the leading hemisphere apex towards the anti-Jupiter facing hemisphere, is
552 an indication of quasi-trapped ions undergoing clockwise drift motion in addition to their bounce
553 motion. In general, ions with larger rigidities have more probability of reaching the surface as they
554 drift around Ganymede.
555
556 Our O^{++} and S^{+++} trajectory simulations corresponding to science case (ii) show the existence of pairs
557 of narrow bands of ion precipitation at low latitudes ($\sim \pm 30°$) extending approximately from 0° to
558 180◦W longitudes (that is the downstream hemisphere). This feature is particularly notable in the
559 populations of initial energy equal to 30 keV (see Figure 5 panel (c) and Figure 6 panel (c)). Such
560 features have been also found in the results of other studies referring to similar conditions as the ones
561 corresponding to our science case (ii) (e.g., Poppe et al. 2018). We believe that these features indicate
562 the presence of quasi-trapped ion populations in Ganymede's closed field line region, as previously
563 proposed by Poppe et al. (2018), in agreement also with the Galileo EPD observations of trapped ion
564 populations (Williams, 2001). Our model results indicate that such radiation belts are populated with
565 ions ejected from the magnetotail, mainly through tail reconnection (e.g., Jia et al. 2010a; Toth et al.
566 2016). Modelling work has shown that the plasma convection in the tail is mainly governed by

567 reconnection, which diverts part of the flow towards Ganymede and the rest downtail into the Jovian
568 flow (Jia et al. 2010a). The flow that returns from the reconnection site towards Ganymede provides
569 the source population of energized plasma, which may be streaming along the field lines and
570 eventually precipitate onto the surface. The narrow precipitation bands evident in Figure 5 and Figure
571 4 correspond to the magnetic footpoints of the open-closed field line boundaries, where particles with
572 relatively small pitch angles can overcome the magnetic mirror force and precipitate to the surface of
573 Ganymede.
574
575 4.4. Sputtering
576
577 The aforementioned results become of particular interest when speculating on the sputtering and
578 surface weathering processes at Ganymede. Energetic Oxygen and Sulphur ions can sputter the icy
579 surface with high efficiency populating the moon's exosphere with H_2O molecules (Johnson 1990).
580 The energetic particle radiation can also activate radiolytic processes in the upper surface layers
581 which are then followed by reactions among the water-dissociation products, resulting in the release
582 of O_2, H_2, and other minor products (Cooper et al. 2001; Moore et al. 2007; Plainaki et al. 2015; Teolis
583 et al. 2017). Contrary to sputtering, radiolysis depends strongly also on the ice temperature. In this
584 work, we investigate the effect of ion precipitation in releasing water molecules directly through
585 sputtering and we discuss our findings and their possible implications to weathering. The effect of
586 Jovian energetic ions in releasing molecules through radiolysis, as well as the detailed generation and
587 evolution of Ganymede's exosphere (see, for instance, Marconi, 2007; Plainaki et al. 2015) goes
588 beyond the scope of the current work and will be treated in a separate paper. Here we discuss some
589 implications of the results of current simulations, in terms of total precipitating flux patterns, on the
590 surface's H_2O-sputtering capacity.
591
592 Figure 9 presents the sputtered-H_2O yields corresponding to Hydrogen, Oxygen and Sulfur ions in a
593 wide energy range, based on recent estimations by Teolis et el. (2017). The sputtering yield is defined
594 here as the number of surface atoms or molecules released per impacting ion; it depends, among
595 others, on the impacting ion's mass, energy, atomic number, and impacting angle, and the surface
596 properties (Famà et al. 2008; Teolis et al. 2017). Taking into consideration our simulation results
597 summarized in Table 2, we estimate the expected sputtering rates corresponding to different incident
598 ions for different science cases. As shown in Table 3, the maximum sputtering rate all over the surface
599 is expected during science case (ii).
600

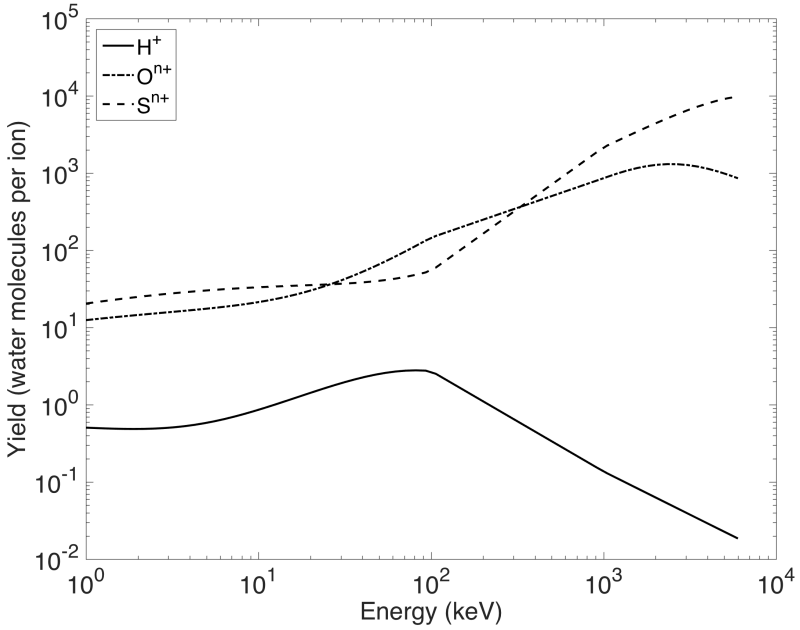

Figure 9: Water release yield due to the precipitation of H^+, O^{n+}, S^{n+} in the energy range 1 keV – 7 MeV. Yield values are from Teolis et al. (2017).

To estimate the average sputtered-water rate, the individual rates corresponding to the three science cases, together with their relative weight during a complete period of the JPS movement upwards and downwards the moon's orbital plane, should be taken into account. We assume here that the average sputtering rate, A, may be given by the following expression:

$$A = \begin{cases} A_{G2} + (A_{G8} - A_{G2}) \cdot |\cos(\omega t)|, & \omega t \in [0\ \pi) \\ A_{G28} + (A_{G8} - A_{G28}) \cdot |\cos(\omega t)|, & \omega t \in [\pi\ 2\pi] \end{cases} \quad (1)$$

where A_{G2} is the total sputtering rate during science case (i), A_{G8} is the total sputtering rate during science case (ii), and A_{G28} is the total sputtering rate during science case (iii) (see Table 3); ω is the angular frequency of the JPS movement, equal to $\omega = \frac{2\pi}{T}$, with T being the Jupiter's rotation period, equal to ~ 9 h 50 min, and t the time.

Averaging A over a complete period of the JPS movement, we find that the average sputtering rate of H_2O-molecules from Ganymede's surface is ~ 2.6×10^{26} s^{-1}.

This estimate is higher than our previous results in Plainaki et al. (2015), approximately by a factor of 3.7. This difference is reasonable and is due to the more extended ion spectrum used in the current paper and the consequent contribution to sputtering of the high energy ions, especially the heavier ones. We note that in the estimates in Plainaki et al. (2015), which referred only to science case (ii)

623 and, the considered impacting magnetospheric ion energy was limited to a maximum of 100 keV.
624 Such an assumption resulted in a lower sputtering rate. Indeed, Figure 9 shows the importance in
625 sputtering of ion energies higher than 100 keV, especially for the Oxygen and Sulfur ion species. Our
626 current estimate is close to the sputtering rate value proposed by Poppe et al. (2018) (7×10^{26} s^{-1})
627 which, however, as the results by Plainaki et al. (2015) referred only to conditions similar to those
628 during the Galileo G8 flyby. For this exact case, the sputtering rate estimates in this study are lower
629 than those in Poppe et al. (2018) by a factor of ~1.6 (see Table 3, middle column). Such differences
630 can be attributed to the different models used in each study and support, even if in an indirect way,
631 that the full-mirroring assumption considered in both Plainaki et al. (2015) and the current paper leads
632 to results that are not extraordinarily different than those in other studies.
633 The average rate of the sputtered mass from Ganymede's surface is estimated to be ~equal to 7.8
634 kg/s. Assuming a direct escape fraction of 16.8% (Plainaki et al. 2015), we estimate a loss of the order
635 of 1.3 kg/s. This value is significantly smaller than the one estimated for Europa, equal to ~50 kg/s
636 (e.g., Schreier et al. 1993; Saur et al. 1998).
637
638 Table 1: Ion fluxes integrated in energy (in cm^{-2} s^{-1}) precipitating to Ganymede's surface according
639 to the simulation results of this work.

Ion species	Science case (i) G2 conditions		Science case (ii) G8 conditions		Science case (iii) G28 conditions	
	Flux (in cm^{-2} s^{-1})		Flux (in cm^{-2} s^{-1})		Flux (in cm^{-2} s^{-1})	
	average	maximum	average	maximum	average	maximum
Hydrogen	2.9×10^{5}	3.9×10^{6}	4.3×10^{6}	2.5×10^{7}	4.1×10^{4}	3.9×10^{5}
Oxygen	1.8×10^{5}	1.1×10^{6}	1.4×10^{6}	5.7×10^{6}	8.0×10^{4}	5.9×10^{5}
Sulphur	2.6×10^{5}	1.4×10^{6}	1.5×10^{6}	5.7×10^{6}	1.4×10^{5}	8.3×10^{5}

640
641 Table 2: Total ion precipitating rate on Ganymede's surface (in s^{-1}).

Ion species	Science case (i) G2 conditions	Science case (ii) G8 conditions	Science case (iii) G28 conditions
	Precipitation rate (in s^{-1})	Precipitation rate (in s^{-1})	Precipitation rate (in s^{-1})
Hydrogen	2.5×10^{23}	3.6×10^{24}	3.2×10^{22}
Oxygen	1.6×10^{23}	1.2×10^{24}	6.9×10^{22}
Sulphur	2.3×10^{23}	1.4×10^{24}	1.2×10^{23}

642

Table 3: Sputtered water rate on Ganymede's surface (in s^{-1}) for different configurations of Ganymede's magnetic field with respect to JPS.

Ion species	Science case (i) G2 conditions	Science case (ii) G8 conditions	Science case (iii) G28 conditions
	Sputtered-water rate (in s^{-1})	Sputtered-water rate (in s^{-1})	Sputtered-water rate (in s^{-1})
Hydrogen	4.7×10^{23}	7.5×10^{24}	4.5×10^{22}
Oxygen	2.7×10^{25}	3.4×10^{26}	9.1×10^{24}
Sulphur	1.2×10^{25}	9.4×10^{25}	5.8×10^{24}
total	3.9×10^{25}	4.4×10^{26}	1.5×10^{25}

4.5. Ion precipitation and weathering

The current study confirms the existence of an equatorial leading/trailing asymmetry in the ion precipitation maps, also during different configurations between Ganymede's magnetic field and JPS. This outcome is consistent with the past-findings of a relatively bright leading hemisphere compared to a darker trailing one (Clark et al. 1986). However, due to the absence of new surface data, our knowledge on the detailed connection between the ion precipitation properties and spectroscopic weathering effects at Ganymede is nowadays limited.

Our results considering science case (ii) are also consistent with the surface albedo dichotomy observed by Voyager and Galileo between the bright polar caps and the relatively dark equatorial region (Smith et al. 1979; Johnson, 1997; Khurana et al. 2007). Khurana et al. (2007) noted that the brightness boundary on Ganymede's surface corresponds closely to the OCFB line and argued that the sputtering and redistribution of water frost takes place onto optically thick material hence resulting in a brightening of the moon's surface albedo. The results of the current paper do not contradict such a scenario, supported also by past simulations by Fatemi et al. (2016) and Poppe et al. (2018). Indeed, our simulations do show a precipitation guided mainly by the OCFB position, however, the border separating the highly accessible regions from the lower latitude ones is not distinct. This happens because the precipitation depends strongly not only on the ion rigidity (depending on the ion species, energy, and charge state) but also on the configuration between Ganymede's magnetic field and the JPS.

669 Ligier et al. (2019) studied the surface composition and properties of Ganymede performing linear
670 spectral mixing modeling of a high spectral resolution dataset, acquired with the near-infrared (1.40–
671 2.50 μm) ground-based integral field spectrometer SINFONI (SINgle Faint Object Near-IR
672 Investigation) of the Very Large Telescope (VLT hereafter) located in Chile. These authors found
673 that the abundance maps of H_2O-ice on Ganymede's surface are characterized by a latitudinal gradient
674 linked to the impact of the external environment. In particular, they found that H_2O-ice is nearly
675 absent around the apex of the trailing hemisphere and tends to be less abundant near the equator (see
676 Ligier et al. (2019), Fig. 10b). Indeed, the abundance maps by Ligier et al. (2019) are well correlated
677 with the heavy ion precipitation patterns we estimate in this paper (see Figures 5 and 6). Moreover,
678 our results confirm that the high latitude surface regions and the leading side of Ganymede are more
679 bombarded by heavy ions than the equatorial regions of the trailing side, also during different
680 configurations between Ganymede's magnetic field and JPS (see Figures 5 and 6). The spatial
681 distribution of the H_2O-sputtering rate is expected to follow the heavy ion precipitation patterns, since
682 the related yield increases with the ion mass (see Figure 8). As a result, the related redistribution of
683 water frost is expected to cause a surface brightening that is well correlated with these ion
684 precipitation patterns. However, at Ganymede, water sublimation is believed to play also an important
685 role in surface water release, maybe the dominant one (Marconi, 2007; Plainaki et al. 2015;
686 Shematovich, 2016). Since sublimation depends strongly on surface temperature, it is expected to
687 preferentially redistribute ice from the equator of the illuminated hemisphere towards the poles. Such
688 a situation, however, would not result in any preferential release of water from the leading side of
689 Ganymede rather than the trailing one, unless sublimation is somehow related also to the morphology
690 of the impinging radiation. Since for a specific temperature ice sublimation will be more efficient at
691 regions where ice is more abundant (see discussion in Marconi (2007)), the removal of the upper
692 layer materials and the exposure (due to sputtering) of fresh ice to sunlight could maximize also the
693 efficiency in sublimated-ice release from the surface. Such a scenario, given the estimated ion
694 precipitation patterns (see Figures 5 and 6), would explain why the trailing equatorial region is more
695 depleted in H_2O-ice than the leading equatorial region. We also note that the high H_2O sublimation
696 rate estimated for Ganymede in past papers (Marconi, 2007; Leblanc et al. 2017; Shematovich 2016)
697 referred to a pure water-ice surface. Whereas Ganymede's surface has long been known to be
698 dominated by H_2O-ice (Kieffer and Smythe, 1974; Pollack et al. 1978; Calvin et al. 1995),
699 Galileo/NIMS observations have evidenced for the first time also the presence of CO_2 frost (McCord
700 et al. 1997, 1998; Hibbitts et al. 2003) which may be hosted in non-icy low-albedo materials like
701 hydrated salts and acids (McCord et al. 1998). Recent spectroscopic observations from ground (Ligier
702 et al. 2019) and from space, e.g. New Horizon/Lorri (Grundy et al. 2007) and Juno/JIRAM (Mura et

al. submitted), have further confirmed the presence and geographical distribution of non-icy materials across the surface of Ganymede. The existence of such materials, at any part of the surface, would hamper the action of ice-sublimation unless some other processes (e.g., sputtering) removed part of the surface upper layers allowing the underlying fresh ice to some to sunlight. For this reason, the leading hemisphere which gets more sputtered with respect to the trailing one, when illuminated, is expected to mostly favour sublimation. Again, this scenario is further supported by the observations by Ligier et al. (2019) who showed that the total H_2O-ice abundance map, composed of the sum of all grain sizes of both amorphous and crystalline H_2O-ices, derived assuming the full grain size distribution and both amorphous and crystalline species, is well anti-correlated to the dark component's abundance map. Of course, other exogenous processes may also play a role in the determination of the surface's brightness, such as ice excavation caused by micrometeoroid bombardment, as previously proposed by Ligier et al. (2019), preferentially occurring on the leading hemisphere (Bottke et al. 2013).

The results of the current study further confirm the asymmetric impact of radiation on the structure of surface water ice. It is believed that the existence of amorphous ice –mostly in the first micrometer layers of Ganymede's surface– is due to higher radiation processing (Hansen and McCord, 2004; Famà et al. 2010). Ligier et al. (2019) found that the amorphous ice distribution has a weakly higher abundance within the polar regions and a depletion in the equatorial trailing side (see their Fig. 10d). Our results confirm that the polar regions (together with the leading equatorial side) are indeed more radiated with respect to rest of the surface. Since the crystallization of water ice is expected to take place faster in the warmer equatorial regions, in the amorphous ice abundance maps in Ligier et al. (2019) large latitudinal differences could not be identified. Last, the strong latitudinal variation in the small grain size distribution by Ligier et al. (2019) (10μm-50μm) seems to follow very well our modelled precipitation maps corresponding to H^+ with initial energies 30-300 keV (see, for instance, Figure 3).

The modelled precipitation of heavy ions is also consistent with the measured distribution of sulfuric acid hydrate on the surface (Ligier et al.2019). The enhanced abundance of this material just where the O^{++} and S^{+++} precipitation flux is more intense, strongly supports its exogenic origin. Anyway, a future detailed study on the surface molecules redistribution after sputtering and consequent effects on the surface optical properties may shed light to this argument. In this view, the current simulations may be used as a starting point for weathering studies when considering the morphology of the surface's bombardment by Jupiter's magnetospheric ions.

5. SUMMARY AND CONCLUDING REMARKS

In this paper we apply a single-particle MC model (Plainaki et al. 2015) driven by the electromagnetic field from a well-established MHD model (Jia et al. 2008, 2009) to investigate the dynamics of the Jovian energetic ions in the near Ganymede space and to estimate the precipitating flux to the moon's surface. For the first time, we perform energetic ion trajectory computations for three distinct configurations between Ganymede and Jupiter's plasma sheet, characterized by magnetic and electric field conditions similar to those during the G2, G8, and G28 flyby of Galileo. The considered initial energies for the ions range from 1 keV to 3 MeV and the spectra given by Paranicas et al. (1999) have been used.

The most important findings of the current work can be summarized as follows:

- The surface precipitation patterns for H^+, O^{++}, S^{+++} show a large-scale dichotomy in surface fluxes between the polar and the lower latitude regions of Ganymede. Longitudinal variations in the width of the equatorial shielded region are observed in the precipitation maps of the considered ion populations, with the widest latitudinal shielding occurring on the trailing hemisphere for ions with low initial rigidity (e.g., low-energy H^+) when Ganymede is below the centre of JPS. The shielding of the equatorial region of the leading hemisphere (plasma downstream) depends not only on the initial rigidity of the ions but also on the magnetic field configuration with respect to JPS.
- When Ganymede is above or below the centre of JPS the Alfvén wings are found to be not perfectly anti-asymmetric. This happens because the magnetic field in the Jupiter and anti-Jupiter facing sides is asymmetric (see also Jia et al. 2008). Regions of very low or zero flux inside the Alfvén wings when Ganymede is above or below the centre of JPS, appear both in the H^+ (see Figure 2) and the heavier ion circulation maps (see, for instance, Figure 7).
- The H^+ circulation and surface precipitation patterns are compatible with a flow guided strongly by the position of the OCFB. A relatively small contribution in the low-latitude surface precipitation on the leading side comes from the magnetotail direction. The H^+ precipitation on Ganymede's polar caps is more extended when Ganymede is above the centre of JPS than when it is below. The low energy-H^+ precipitation on high-latitude/polar caps surface regions present a significant asymmetry between the Jupiter and the anti-Jupiter facing sides when Ganymede is above or below the centre of JPS. Such an asymmetry is in the opposite sense for the case that the moon is above or below the centre of JPS, and for the

Northern and Southern hemispheres. This high-latitude/polar caps asymmetry is attenuated when Ganymede is near the centre of JPS. In this case the total precipitating flux is higher.

- Features indicating the presence of quasi-trapped ion populations in Ganymede's closed field line region, as previously proposed by Poppe et al. (2018) and in agreement also with the Galileo EPD observations (Williams, 2001), have been found in the O^{++} and S^{+++} precipitation maps corresponding to science case (ii). These features are found at low latitudes ($\sim \pm 30^{o}$) of the downstream hemisphere and they are particularly notable in the populations of initial energy equal to 30 keV (see Figure 5 panel (c) and Figure 6 panel (c)). They correspond to the magnetic footpoints of the open-closed field line boundaries.
- The surface precipitation of Oxygen ions depends strongly on their actual charge state. The O^{++} precipitation patterns are also compatible with a flow through the polar caps and a mounting of the ions in the downstream magnetotail region. The exact morphology depends strongly on the configuration of Ganymede's magnetic field with respect to JPS. The O^{++} flow gains access mainly through the OCFB region; in the magnetotail, ions are redirected along the closed field lines back to Ganymede's surface (see Figures 5 and 6), mainly through tail reconnection (e.g., Jia et al. 2010a; Toth et al. 2016). A similar situation is observed also in the simulation results considering the S^{+++} case (see Figure 7). This phenomenon may be of interest from a comparative planetary space weather perspective.
- Current simulations show that the overall precipitation is more intense when Ganymede is near the centre of JPS. The low-latitude/equatorial surface precipitation flux appears always more intense in the anti-Jupiter direction, at least for initial ion energies lower than 300 keV. This shift of the maximum equatorial precipitation away from the leading hemisphere apex towards the anti-Jupiter facing hemisphere, may be an indication of quasi-trapped ions undergoing clockwise drift motion in addition to their bounce motion. We conclude, therefore, that the access of JPS ions to Ganymede's surface is permanently antisymmetric between the Jupiter and anti-Jupiter facing hemispheres, with detailed characteristics that depend strongly on the moon's position with respect to JPS and the ion rigidities.
- The average sputtering rate of H_2O-molecules from Ganymede's surface over a complete period of the JPS movement up and down the moon is $\sim 2.6\times10^{26}$ s^{-1}. The spatial distribution of the H_2O-sputtering rate is expected to follow well the heavy ion precipitation patterns, since the related yield increases with the ion mass. The heavy ion precipitation patterns estimated in this paper are well correlated with water abundance maps produced on the basis of SINFONI/VLT/ESO observations (Ligier et al. 2019) indicating that H_2O-ice is nearly absent around the apex of the trailing hemisphere and tends to be less abundant near the equator.

The results of the current work may help to better understand the nature of ion-moon interactions in Jupiter's magnetosphere, their dynamic behaviour, and the related implications from a planetary space weather perspective. However, further theoretical work focusing on the study of reconnection and particle acceleration inside Ganymede's magnetosphere is necessary to shed light in the processes characterizing the ion-moon interactions. Recent efforts (e.g., Kaweeyanun et al. 2020) showed that the average reconnection rate is a function of Ganymede's position along its orbit around Jupiter, being driven by Jupiter's rotation. Future joint-analysis of such effects on the ion precipitation on Ganymede's surface would be very important in order to have more accurate predictions of the related surface signatures, in preparation for the JUICE mission of ESA (Grasset et al. 2013).

Particle precipitation may be considered as the key parameter determining sputtering of water molecules, an important exosphere source for the Galilean satellites (e.g.: Shematovich et al. 2005; Plainaki et al. 2012; Shematovich, 2016 and references therein). Its variability has direct impacts also on the exosphere generation and evolution. Knowledge on the joint-system of Jupiter's magnetosphere and Ganymede's environment (magnetosphere-exosphere-surface) is of significant importance during the design of future missions to this Galilean moon and the planning of the observations (see, for example, discussion in Plainaki et al. 2016). Knowledge on planetary space weather in the context of Outer Solar System exploration is necessary also for the related environment specification studies and definition of possible countermeasures.

References

Allioux, R., Louarn, P., & André, N. 2013, AdSR, 51, 1204

André, N., Grande, M., Achilleos, N., et al. 2018, P&SS, 150, 50, DOI: 10.1016/j.pss.2017.04.020

Bagenal, F., Wilson, R. J., Siler, S., et al. 2016., JGRE, 121, 871, doi:10.1002/2016JE005009

Boris, J.P. 1970, MATT-769 Technical Report (4168374), NSA-24-023976 (Princeton Univ., N. J. Plasma Physics Lab.)

Calvin, W.M., Clark, R.N., Brown, R.H., et al. 1995, JGR, 100, 9, 19041

Carnielli, G., Galand, M., Leblanc, F., et al. 2019, Icarus, 330, 42, doi:10.1016/j.icarus.2019.04.016

Carnielli, G., Galand, M., Leblanc, F., et al. 2020, Icarus, doi: 10.1016/j.icarus.2020.113691

Chen, J., & Palmadesso, P. J. 1986, JGR, 91(A2), 1499

Clark, R. N., Fanale, F. P., & Gaffey, M. J. 1986, in Some background about satellites, ed. J. A. Burns & M. S. Matthews, IAU Colloq. 77 (Tuscon: University of Arizona Press), 437

837 Collier, M. R., Hamilton, D. C., 1995. The relationship between kappa and temperature in energetic
838 ion spectra at Jupiter, Geophysical Research Letters, 22(3), 303–306.
839 Collinson, G., Paterson, W. R., & Bard, C., et al. 2018, GeoRL, 45, 3382, doi:
840 10.1002/2017GL075487
841 Cooper, J.F., Johnson, R.E., Mauk, B.H., et al. 2001, Icarus 149, 133
842 Dorelli, J. C., Glocer, A., Collinson, G., et al. 2015, JGRA, 120, 5377, doi:10.1002/2014JA020951
843 Famà, M., Loeffler, M. J., Raut, U., et al. 2010, Icarus, 207, 314
844 Fatemi, S., Poppe, A. R., Khurana, K. K., et al. 2016, GeoRL, 43, 4745–4754,
845 doi:10.1002/2016GL068363
846 Frank, L. A., Paterson, W. R., Ackerson, K. L., et al. 1997, GeoRL, 24(17), 2151
847 Gomis, O., Satorre, M. A., Strazzulla, G., et al. 2004, P&SS, 52, 371
848 Grasset, O., Dougherty, M.K., Coustenis, A., et al. 2013, P&SS, 78, 1, doi:10.1016/j.pss.2012.12.002
849 Grundy, W., Buratti, B. Cheng, A., et al. 2007, Science, 318, 234, doi: 10.1126/science.1147623
850 Gurnett, D.A., Kurth, W.S., Roux, A., et al. 1996, Nature, 384, 535, doi:10.1038/384535a0
851 Hall, D.T., Feldman, P.D., McGrath, M.A., et al. 1998, ApJ, 499, 475, doi: 10.1086/305604
852 Hansen, G. B., & McCord, T. B. 2004, JGR, 109, E01012, doi:10.1029/2003JE002149
853 Hibbitts, C.A., Pappalardo, R.T., Hansen, G.B., et al. 2003, JGR, 108 (5), 5036
854 Jia, X., Walker, R. J., Kivelson, M. G., et al. 2008, JGR, 113, A06212, doi:10. 1029/2007JA012748
855 Jia, X., Walker, R. J., Kivelson, M. G., et al. 2009, JGR, 114, A09209, doi:10.1029/2009JA014375
856 Jia, X., Walker, R. J., Kivelson, M. G., et al. 2010a, JGRA, 115, A12202,
857 doi:10.1029/2010JA015771
858 Jia, X., Kivelson, M. G., Khurana, K. K., et al. 2010b, SSRv, 152, 271, doi:10.1007/s11214-009-
859 9507-8
860 Johnson R. E. 1990, Energetic Charged-Particle Interactions with Atmospheres and Surfaces
861 (Springer-Verlag Berlin Heidelberg ed.), doi: 10.1007/978-3-642-48375-2
862 Johnson, R. E. 1997, Polar “Caps” on Ganymede and Io revisited, Icarus, 128, 469
863 Johnson, R. E., Carlson, R. W., Cooper, J. F., et al. 2004, in Jupiter: The planet, satellites, and
864 magnetosphere, ed. R. E. Johnson et al. (Cambridge, UK: Cambridge University Press), 483
865 Khurana, K. K., & Pappalardo, R. T., et al. 2007, Icarus, 191, 193
866 Keppler, E., & Krupp, N. 1996, P&SS, 44(2), 71
867 Kieffer, H.H., & Smythe, W.D. 1974, Icarus, 21, 506
868 Kivelson, M. G., Warnecke, J., Bennett, L., et al. 1998, JGR, 103(E9), 19, 963
869 Kivelson, M. G., Bagenal, F., Kurth, W. S., et al. 2004, in Jupiter: The planet, satellites, and
870 magnetosphere, ed. R. E. Johnson et al. (Cambridge, UK: Cambridge University Press), 513

871 Kivelson, M. G., Khurana, K. K., Russell, C. T., et al. 1996, Nature, 384, 537, doi:10.1038/384537a0
872 Kivelson, M.G. ,Khurana, K.K., Coroniti, F.V., et al. 1997, GeoRL, 24, 2155, doi:10.1029/97GL02201
873 Kliore, A.J. 1998, Highlights Astron. 11, 1065
874 Kaweeyanun, N., Masters, A., Jia, X. 2020, GeoRL, 47, e2019GL086228,
875 doi:10.1029/2019GL086228
876 Ligier, N., Paranicas, C., Carter, J., et al. 2019, Icarus 333, 496, doi:10.1016/j.icarus.2019.06.013
877 Marconi, M.L. 2007, Icarus, 190, 155, doi:10.1016/j.icarus.2007.02.016
878 Mauk, B. H., Mitchell, D. G., McEntire, R. W., et al. 2004, JGR, 109, A09S12,
879 doi:10.1029/2003JA010270
880 McCord, T.B., Carlson, R.W., Smythe, W.D., et al. 1997, Science, 278, 271
881 McCord, T.B., Hansen, G.B., Clark, R.N. et al. 1998, JGR, 103, E4, 8603
882 McGrath, M.A., Xianzhe, J., Retherford, K., et al. 2013, JGRA, 118 (5), 2043
883 Mura, A., Adriani, A., Sordini, R., et al. 2020, submitted
884 Paranicas, C., Paterson, W. R., Cheng, A. F., et al. 1999, JGR, 104, 17459
885 Paty, C., Paterson, W., Winglee, R. 2008, JGR, 113, A06211, doi:10.1029/2007JA012848
886 Paty, C., & Winglee, R. 2004, GeoRL, 31, L24806, doi:10.1029/2004GL021220
887 Paty, C., & Winglee, R. 2006, GeoRL, 33, L10106, doi:10.1029/2005GL025273
888 Plainaki, C., Milillo, A., Massetti, S., et al. 2015, Icarus, 245, 306, doi: 10.1016/j.icarus.2014.09.018
889 Plainaki, C., Lilensten, J., Radioti, A., et al. 2016, JSWSC, 6, A31, 2016, doi:10.1051/swsc/2016024
890 Plainaki, C., Cassidy, T.A., Shematovich, V.I., et al. 2018, SSRv, 214, 40, doi: 10.1007/s11214-018-
891 0469-6
892 Plainaki, C., Sindoni, G., Grassi, D., et al. 2020, PSS, P&SS, under review
893 Pollack, J.B., Witteborn, F.C., Erickson, E.F., et al. 1978, Icarus 36, 271
894 Poppe, A. R., Fatemi, S., Khurana, K. K. 2018, JGRA, 123, 4614, doi:10.1029/2018JA025312
895 Shay, M. A., & Swisdak, M. 2004, PhRvL, 93, 1, doi:10.1103/PhysRevLett.93.175001
896 Shematovich, V.I. 2016, SoSyR, 50, 4, 262–280, doi:10.1134/S0038094616040067
897 Shi, M., Baragiola, R. A., Grosjean, D. E., et al. 1995, JGR, 100(E12), 26, 387–26, 395
898 Smith, B. A., Soderblom, L. A., Beebe, R., et al. 1979, Science, 206(4421), 927
899 Teolis, B. D., Plainaki, C., Cassidy, T. A., et al. 2017, JGRE, 122, 1996, doi:10.1002/2017JE005285
900 Turc, L., Leclercq, L., Leblanc, F., et al. 2014, Icarus, 229, 157, doi:10.1016/j.icarus.2013.11.005
901 Toth, G., Jia, X., Markidis, S., et al. 2016, JGRA, 121, 1273, doi:10.1002/2015JA021997
902 Williams, D.J., Mauk, B.H., McEntire, R.W., et al. 1997, GeoRL, 24(17), 2163
903 Williams, D.J. 2001, GeoRL, 28(19), 3793
904 Williams, D. J., McEntire, R. W., Jaskulek, S., et al. 1992, SSRv, 60, 385

905 Williams, D. J., Mauk, B., & McEntire, R. W. 1997, GeoRL, 24(23), 2,953
906 Zhou, H., Toth, G., Jia, X., et al. 2019, JGRA, doi:10.1029/2019JA026643